Microfluid Nanofluid (2008) 4:375–389
DOI 10.1007/s10404-007-0188-x

RESEARCH PAPER

A rapid magnetic particle driven micromixer

Yiou Wang · Jiang Zhe · Benjamin T. F. Chung · Prashanta Dutta

Received: 21 February 2007 / Accepted: 21 May 2007 / Published online: 30 June 2007
© Springer-Verlag 2007

Abstract Performances of a magnetic particle driven micromixer are predicted numerically. This micromixer takes advantages of mixing enhancements induced by alternating actuation of magnetic particles suspended in the fluid. Effects of magnetic actuation force, switching frequency and channel's lateral dimension have been investigated. Numerical results show that the magnetic particle actuation at an appropriate frequency causes effective mixing and the optimum switching frequency depends on the channel's lateral dimension and the applied magnetic force. The maximum efficiency is obtained at a relatively high operating frequency for large magnetic actuation forces and narrow microchannels. If the magnetic particles are actuated with a much higher or lower frequency than the optimum switching frequency, they tend to add limited agitation to the fluid flow and do not enhance the mixing significantly. The optimum switching frequency obtained from the present numerical prediction is in good agreement with the theoretical analysis. The proposed mixing scheme not only provides an excellent mixing, even in simple microchannel, but also can be easily applied to lab-on-a-chip applications with a pair of external electromagnets.

Y. Wang · J. Zhe (✉) · B. T. F. Chung
Department of Mechanical Engineering,
The University of Akron,
Akron, OH 44325-3903, USA
e-mail: jzhe@uakron.edu

P. Dutta
School of Mechanical and Materials Engineering,
Washington State University,
Pullman, WA 99164-2920, USA

Keywords Magnetic particles · Micromixing · Microfluidic · Magnetic actuation

List of symbols

A	cross-section area of the microchannel (m^2)
A_p	cross-section area of the particle (m^2)
B	magnetic flux density (Tesla)
C	dimensionless concentration
C_D	drag coefficient
D	diffusion coefficient (m^2/s)
F	force (N)
f	switching frequency (Hz)
f_{cr}	critical switching frequency (Hz)
H	channel height (m)
H_e	magnetic field strength (A/m)
H_M	electromagnet thickness (m)
I	current (A)
L	streamwise dimension or length (m)
m	particle mass (kg)
M	magnetization of the particle (A/m)
P	pressure (N/m^2)
Pe	peclet number ($ReSc$)
r	particle radius (m)
Re	Reynolds number ($UW\rho_f/\eta$)
Sc	Schmidt number ($\eta/\rho_f D$)
St	Strouhal number (Wf/U)
S	distance between two parallel electromagnets (m)
t	time (s)
T	period, $1/f$ (s)
U	relative velocity between the fluid and particle along y direction (m/s)
V	volume (m^3)
$\vec{V}$	fluid's velocity vector
$\vec{v}$	particles' velocity vector
W	lateral dimension or width (m)

x streamwise coordinate of the microchannel
y lateral coordinate of the microchannel
z coordinate in the direction normal to the x–y plane

Greek

η dynamic viscosity of the fluid (kg/m s)
ρ density (kg/m^3)
χ magnetic susceptibility of the particle
η_e mixing efficiency (%)
μ permeability (N/A^2)

Subscript

d drag
f fluid
m magnetic
M electromagnet
o prior mixing stage or medium
p particle
r relative
s magnetization saturation
∞ complete mixing state

1 Introduction

Rapid mixing of two or more analytes is essential for many microfluidic systems used in biochemical analysis, immunoassays, and DNA analysis. Rapid mixing is also necessary for microreactors that involve complex chemical synthesis. However, in most microfluidic systems, the flow is laminar with very low Reynolds number; the mixing is dominated by the diffusion. In the absence of turbulent flow, complete and homogeneous mixing of fluids might take very long time, and requires large channel length. In particular, for analyte solutions containing large molecules such as DNA and proteins, the mixing of two solutions becomes very inefficient because the diffusion coefficients are in the order of 10^{-10} m^2/s or less.

Numerous micromixers have been designed in order to enhance the micromixing. These micro mixers fall into two categories, namely, active mixers and passive mixers. Passive mixers have no moving parts, and achieve mixing by virtue of their structure or topology alone. Using passive structures, the fluids are forced to change directions, split or reunify, to increase the contact areas of the sub-streams (Bessoth et al. 1999; Hong et al. 2004; Losey et al. 2002; Mengeaud et al. 2002). As the microchannel dimensions are scaled down to smaller values, larger flow impedance will be generated, which lead to significantly lower flow rate. So far, most passive mixers reported only show relatively high mixing efficiency at low flow rate. Active mixers, however, can produce excellent micromixing by incorporating external energy in the flow. A variety of active mixing schemes have been studied in microfluidic devices to enhance the mixing efficiency. These include ultrasonic excitation (Yang et al. 2001), mechanical stirrers (Lu et al. 2002; Ryu et al. 2004), thermal bubble mixing (Tsai and Lin 2002), dielectrophoretic mixing (Deval et al. 2002), bubble acoustic agitation (Liu et al. 2002), shear superposition micromixer (Bottausci et al. 2004), etc. While active micromixers can produce excellent mixing, they are often difficult to operate, fabricate or integrate to microfluidic chips. Electrokinetic mixers are favorable among active micromixers because of their simplicity and ease of integration to microfluidic chips (Biddiss et al. 2004; Jacobson et al 1999; Oddy et al. 2001; Santiago 2001; Wang et al. 2007; Xuan and Li 2005). However, they require the use of high electrical potentials, which may cause significant impair to the cells or bioorganisms (McClain et al. 2001).

Active micromixers utilizing magnetic forces represent another important class of mixing possibility (Hessel et al. 2005; Nguyen et al. 2005). Although magnetic microstirrers enable efficient mixing, they typically involve moving parts and are difficult to package and seal (Lu et al. 2002; Ryu et al. 2004). Magneto-hydro-dynamics (MHD) micromixers (West et al. 2002) utilize Lorentz force to agitate fluids and induce secondary complex chaotic flows. However, Lorentz force is proportional to the fluid volume, as the microchannel dimensions are scaled down to smaller values, the agitation force is too small to induce sufficient chaos. In addition, MHD mixers can only be used for conductive fluids.

Recently magnetic particle actuation has received great interest because of its potential application in the field of micro biological assay system (Pamme 2006; Zborowski et al. 1999). The sub-streams containing target molecules and the magnetic particles are mixed so that target cells or molecules are specifically bonded to magnetic beads coated with antibody (Hayes et al. 2001). Consequently the magnetically labeled biomolecules can be separated and analyzed. Mixing of fluids containing magnetic beads and biological solutions are critical for the microfluidic devices targeted at these applications. Actuated by magnetic forces, the suspended magnetic particles can add agitation and chaotic advection in the fluid flow and thus enhance the mixing (Rida and Gijs 2004a; Suzuki et al. 2004). Typically, there are two ways to actuate magnetic particles: (1) use of on-chip planar electrodes or 3D micro electromagnets, (2) use of macro-sized external permanent magnet or electromagnet. Suzuki et al. (2004) developed a magnetic micromixer with embedded planar electrodes

at the bottom of the channel. With the weak magnetic field generated by these planar electrodes, the induced chaotic advection is small and the enhancement of the micromixing is limited. To increase the magnetic force, one has to fabricate large aspect ratio planar electrodes to carry a large current. Zolgharni et al. (2007) designed a micromixer using embedded serpentine electrodes with a cross section of 50 μm (height) by 25 μm (width). A maximum mixing efficiency of 85% was predicted at an applied current of 750 mA. However, large aspect ratio planar electrodes for carrying a large electric current will need complicated microfabrication process, and will cause large heat dissipation to the fluid. Another way to generate large magnetic actuation forces is to fabricate 3D micro magnetic actuation structures (Rida and Gijs 2004a, b; Rong et al. 2003). The magnetic actuation structure developed by Rida and Gijs not only creates large agitation forces but also provides a modulated magnetic field in the streamwise direction, which can retain magnetic particle in the microchannel longer and, hence, further enhance the micromixing. However, the fabrication of this micromixer is complicated. To circumvent this problem, macro-sized external electromagnets are chosen for this study, which are commonly used in cell sorting and separation applications (Zborowski et al. 1999). In this paper a magnetic particle driven micromixer with a simple actuation configuration is studied numerically. This micromixer takes advantages of mixing enhancements induced by time-dependent magnetic particle actuation. In order to obtain a high mixing performance, the effects of magnetic force and switching frequency of magnetic field are investigated. Unlike the superposition method utilized by Suzuki et al. (2004), a multi-physics model that simultaneously solves the magnetic particle motion and fluid flow is utilized in this study.

2 Principle and design of the magnetic micromixer

Figure 1a shows the schematic view of a magnetic micromixer considered in this study. The magnetic micromixer consists of a pair of macro-sized external electromagnets that are placed to face each other vertically, and a microchannel located in the middle of the two electromagnets. Application of current to one electromagnet creates large magnetic force and magnetic gradients in the microchannel. When magnetic particles are loaded to the microchannel, they are polarized and subjected to the magnetic forces in the lateral direction (y-direction, parallel to the gravity direction) by the external magnetic field. The magnetic forces actuate the magnetic particles to move in the y-direction of the microchannel. When this electromagnet is switched off and the other electromagnet is turned on, the magnetic forces on the particles change directions and drive the particles to move to the reverse direction. By switching the electromagnets on and off alternatively as shown in Fig. 1b, one can generate periodic magnetic forces that agitate the magnetic particles to oscillate along the y-direction of the microchannel. The mixing in the microchannel is thus improved due to the interaction of the fluids and magnetic particles.

Each electromagnet can be formed by winding copper wires (0.1 mm in diameter, 80 coil turns) on a 99.95% pure iron core. The relative permeability of the electromagnet is approximately 1.3×10^4 (ASM Committee on Magnetically Soft Materials 1964) when the applied magnetic field H_e is in the range of 0.2–2 Oe, which is the case in our study. The usage of the iron core is to magnify the magnetic field by its relative permeability in the vicinity of the electromagnet. The electromagnet considered here is 8 mm long quadrangular whose cross section is 2 cm × 2 cm, and is much larger than the microchannel. The microchannel is placed in the middle between these two electromagnets, and is 1.0 cm (S) away from the pole of each electromagnet. The microchannel under consideration is sketched in Fig. 1c. Two fluids are loaded into the mixing channel through two inlet channels (not shown in the figure) connected to the horizontal mixing channel. Inlet 1 brings buffer solution of scalar concentration $C = 0$, while inlet 2 feeds sample solution of scalar concentration $C = 1$ with seeded magnetic particles. By switching (on and off) current to the two electromagnets alternatively, we are able to apply time dependent agitation forces that induce the oscillation of the magnetic particles in the mixing region. In this work, the computational domain will be the micromixing channel. The streamwise dimension of the microchannel is $L = 1{,}000$ μm and the dimension perpendicular to the x–y plane is $H = 100$ μm. The microchannel's lateral dimension, W is varied from 100 to 300 μm.

3 Magnetic force calculation

The magnetic force exerted on the magnetic particles can be calculated by the following equation:

$$\vec{F}_m = V_p(\vec{M} \cdot \nabla)\vec{B} \tag{1}$$

where $\vec{F}_m$ is the magnetic force, V_p is the particle volume, $\vec{M}$ is the magnetization of the particle, and $\vec{B}$ is the flux density generated by the external electromagnets. Equation (1) indicates that a large magnetization and magnetic flux density are needed to obtain a large magnetic force. Paramagnetic particles CM-10-10 (from Spherotech Inc.), a soft magnetic material particle, are considered in this study.

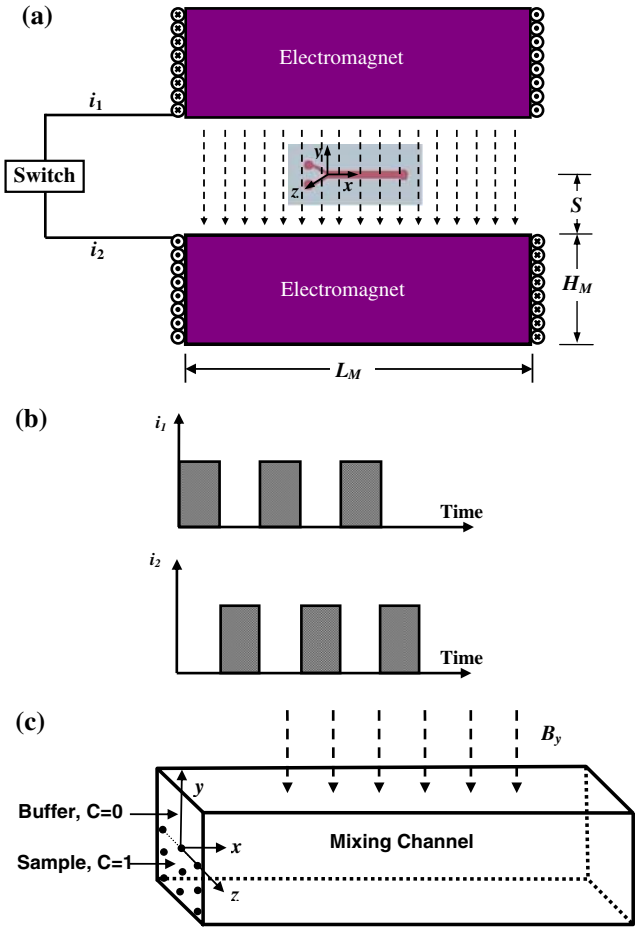

Fig. 1 Schematic diagram of **a** magnetic micromixer; **b** time-dependent current applied to the electromagnets; **c** mixing microchannel

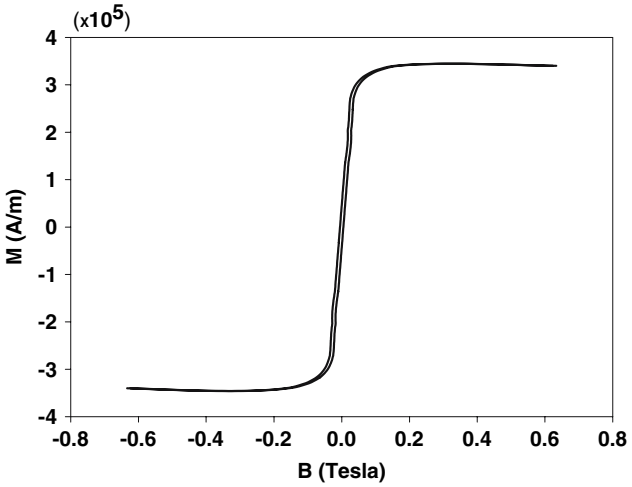

Fig. 2 Hysteresis loop for the paramagnetic particles (Spherotech CM-10-10). Redrawn based on the original B-H hysteresis loop provided by Spherotech, Inc

These paramagnetic particles are selected because they have high saturation magnetization and they are commonly used in the micro cell sorting applications (Suzuki et al. 2004). The hysteresis loop of the paramagnetic particles is illustrated in Fig. 2, which consists of a linear region and a saturation region. In the linear region where the external magnetic field is weak ($B < 0.06\ T$), the magnetization is proportional to the magnetic field. In the saturation region where a strong magnetic field is applied ($B > 0.06\ T$), the magnetization reaches saturation and can be considered a constant ($M_s = 3.363 \times 10^5$ A/m). Here we use electromagnets to generate a strong magnetic field in y direction ($B_y > 0.06\ T$). Note that the other two components B_x and B_z are negligible compared to B_y under the current configuration as described later. Thus the suspended particles are saturated in the y-direction with a constant magnitude M_s. The properties of the paramagnetic particles are listed in Table 1.

The magnetic field generated by the electromagnet is calculated by CFD-ACE+ (ESI Group, Huntsville, AL). Figure 3a shows the numerical results of the nondimensional B_x, B_y and B_z along the centerline that connects the two magnetic poles (y-direction), when the applied current is 50 mA. B_x, B_y and B_z are normalized by the magnetic field B_M at the surface of the electromagnet, which is 2.27 Tesla in this case. For convenience, we defined a separate Cartesian coordinate x_1, y_1, z_1 as shown in Fig. 3a, where $x_1 = x, y_1 = y - S - H_M/2, z_1 = z$. The electromagnet width L_M = 2 cm is used as the reference to normalize the axis. To validate the magnetic flux density calculation by CFD-ACE+, the analytical solution of nondimensional B_y (Furlani 2001) along the axis of a rectangular electromagnet (8 mm long, 2 cm wide and 2 cm thick) is also shown in Fig. 3a. The analytical solution and numerical solution are found to be in excellent agreement.

The magnetic field at the microchannel location is presented in the inset of Fig. 3a for clarity. It is obvious that in the mixing region B_y is dominant, and B_x and B_z can be neglected. Hence the magnetic actuation forces in the x- and z-directions (F_{mx} and F_{mz}) are negligible. Considering the magnetization saturation in the y-direction, Eq. 1 can be simplified as:

Table 1 Property of the magnetic particles CM-10-10

Susceptibility of the particle	χ_p	11.3
Particle radius	r_p	0.5×10^{-6} m
Particle volume	V_p	5.236×10^{-19} m^3
Particle density	ρ_p	1,580 kg/m^3
Particle mass	m_p	8.27×10^{-16} kg

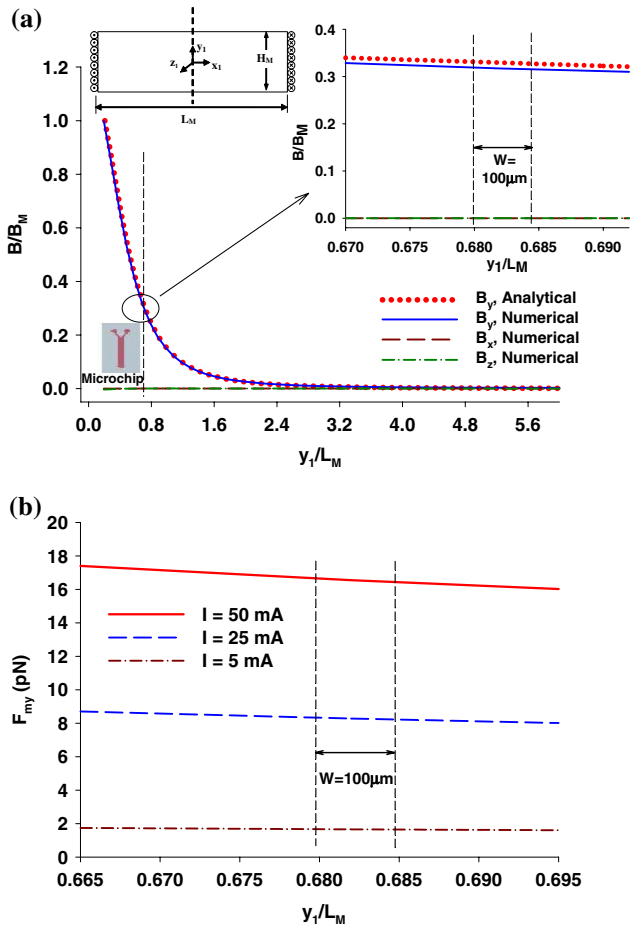

Fig. 3 **a** Magnetic flux density generated by the electromagnet along the centerline that connects the two magnetic poles (z = 0). The analytical solution is based on a rectangular electromagnet (2 cm × 2 cm × 0.8 cm), The baseline B_M is 2.27 Tesla and 2.4 Tesla for numerical and analytical solutions, respectively. Here, $x_1 = x, y_1 = y - S - H_M/2, z_1 = z$. **b** Magnetic actuation force exerted on the particles along the channel length

$$F_{my} = V_p M_s \frac{\partial B_y}{\partial y} \tag{2}$$

where M_s is the saturation magnetization of the particle. Figure 3b shows the magnetic actuation force along the channel's lateral direction (y-direction), showing a slight decrease from 16.64 to 16.46 pN across the microchannel. Because of the usage of large electromagnets, the magnetic actuation forces do not vary along the channel length and the channel height. The resulting magnetic actuation forces are also presented for an applied current of 25 and 5 mA. To simplify the model, the applied actuation forces on magnetic particles are considered constant in the microchannel and are imported to the particle motion equation. It is worth to note here that although the magnetic field/force calculation is based on the specific electromagnets, it is possible to generate 1–100 pN magnetic actuation forces on magnetic particles using the configuration similar to the one shown in Fig. 1 (Gijs 2004; Pamme 2006).

4 Mathematic model and boundary conditions

4.1 Mathematical model

The behavior of incompressible liquid is governed by the continuity and modified Navier-Stokes equations:

$$\nabla \cdot \vec{V} = 0 \tag{3}$$

$$\rho_f \left(\frac{\partial \vec{V}}{\partial t} + (\vec{V} \cdot \nabla)\vec{V} \right) = -\nabla P + \eta \nabla^2 \vec{V} + \vec{F}_d(\vec{r}, t) \tag{4}$$

where $\vec{F}_d(\vec{r}, t)$ is the drag force exerted by the magnetic particles, and is dependent on time t and position $\vec{r}(x, y, z)$; $\vec{V}$ is the velocity vector of fluids; ρ_f is the density of fluid; P is the pressure and η is the dynamic viscosity of the fluid. The motion of the magnetic particles is governed by the Newton's second law:

$$m_p \frac{d\vec{v}}{dt} = \vec{F}_d + m_p \vec{g} + \vec{F}_m \tag{5}$$

where

$$\vec{F}_d = C_D \rho_f (\vec{V} - \vec{v}) \left| \vec{V} - \vec{v} \right| \frac{A_p}{2}. \tag{6}$$

In our work, $\vec{F}_m$ is significant only along the y direction, i.e., only F_{my} exists. C_D is the drag coefficient; $\vec{V}$ is the velocity vector of the magnetic particles and A_p is the cross-section area of the particles. The calculation of the applied magnetic field and force has been described in Sect. 3. The gravity force of each magnetic particle is 8.1×10^{-3} pN. In comparison to the magnetic actuation forces considered in this study (1.66 pN–16.6 pN), the gravity force is neglected in Eq. 5.

The mass transport equation of the sample and buffer is described as:

$$\frac{\partial C}{\partial t} + \vec{V} \cdot \nabla C = D \nabla^2 C \tag{7}$$

where C is the dimensionless concentration. To evaluate the mixing rate at a particular cross-section, a parameter called mixing efficiency (η_e) is defined as the following:

$$\eta_e = \left(1 - \frac{\int_{-A/2}^{A/2} |C - C_\infty| dA}{\int_{-A/2}^{A/2} |C_0 - C_\infty| dA} \right) \times 100\% \tag{8}$$

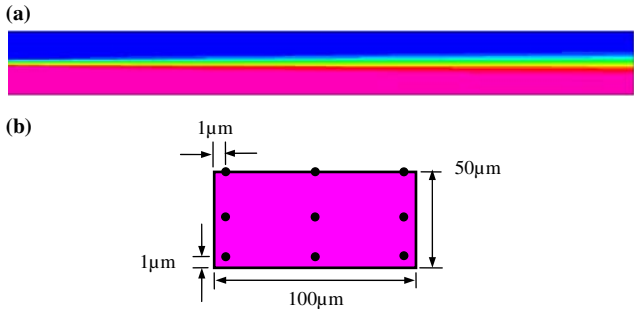

Fig. 4 **a** The fully developed concentration field is used as the initial condition for the subsequent numerical studies; **b** initial positions of particles in the computational domain. The magnetic force is parallel to the gravity force direction

where A is the cross section area of the microchannel, C_∞ is the concentration at the ideal (complete) mixing at the outlet, which is 0.5 for our case, and C_0 is the concentration at the inlets for completely unmixed buffer or sample (0 or 1).

4.2 Boundary conditions and initial conditions

The computational domain is L (streamwise direction) × W (lateral direction) × H (direction normal to x–y plane), where L = 1,000 μm, H = 100 μm and W varies from 100 to 300 μm. At the inlet of the mixing microchannel, both the buffer and sample fluids enter the microchannel (see Fig. 1a) with same inlet velocity at 1 mm/s. The mixing of the two fluids takes place in the microchannel by diffusion only. The fully developed fluid flow field and concentration (Fig. 4a) by diffusion are set as the initial conditions for the subsequent numerical studies. No-slip boundary conditions are applied on all channel walls. At the channel outlet, the atmospheric pressure $P = P_0$ is applied. At $t < 0$, no particles are loaded to the microchannel. To simulate that the particles are uniformly distributed in the sample fluids, starting from $t = 0$ the particles (red dots) are injected from the nine locations of the bottom half channel. As represented in Fig. 4b, all peripheral locations where particles are injected are 1 μm away from the channel wall. The particle's mass flow rate is set at 9×10^{-12} kg/s (volume flow rate: 5.7×10^{-15} m^3/s). This is converted to a volume ratio of 0.057% for the microchannel considered in this study. The initial velocities of the magnetic particles are the same as the sample solution.

5 Numerical scheme and validation

5.1 Numerical scheme

Superposition method is typically adopted to solve the motion of the magnetic particles in the fluid (Suzuki et al. 2004), i.e., the flow velocity field is solved first and then the particle velocity relative to the fluid flow is calculated using Stokes equation. The two velocities are superimposed to obtain the particle trajectory assuming the motion of the magnetic particles does not affect the fluid field. This model tends to have larger errors if a large number of magnetic particles are used because the oscillation of many magnetic particles induces the lateral velocity of the fluid, which causes the enhancement of the micromixing. In our numerical work, we simulated the mixing by solving magnetic particle equations and flow equations simultaneously. Each particle's initial position and velocity are specified. After the particle enters the actuation region, its trajectory and the fluid flow field will be coupled due to the drag force between them. The solution procedure of this coupling problem is given by the flow chart in Fig. 5a. The Spray module of CFD-ACE+ is utilized for the numerical work. Details of the Spray module can be obtained from references (Crocker et al. 2001) and (CFD-ACE+ V2006 help documentation, Spray module). Recently Spray module has been used in numerical simulation of spray combustion (Crocker et al. 2001) and chemical vapor deposition process (Bouteville 2005). The flow chart of the numerical scheme is sketched in Fig. 5b.

5.2 Model validation

5.2.1 Comparison to the theoretical solution

For validation study, a 1-μm single paramagnetic particle (properties are listed in Table 1) is injected from the lower left corner of a straight microchannel and is actuated by a magnetic field perpendicular to the flow direction, as shown in Fig. 6a. The dimensions of the 2D microchannel are L = 1,000 μm and W = 100 μm. This model has an analytical solution (Berthier and Silberzan 2006) with the following assumptions:

(a) Fluid flow field is not affected by the presence of a magnetic particle because of the limited agitation by a single particle.
(b) External magnetic field and gradient are only along the channel's lateral direction (y direction), so is the magnetic force. In our study, we apply $B_y = \sqrt{2(y + 50 \times 10^{-6})}$,

where y is measured in meter. We assume that the properties of the carrier electrolyte fluids are the same as that of water, which are listed in Table 2. The inlet velocity is set at 1 mm/s. To simplify the model, gravity force of the magnetic particles is neglected in both the analytical solution and the numerical work.

Based on above assumptions, the fluid velocity between two parallel plates is

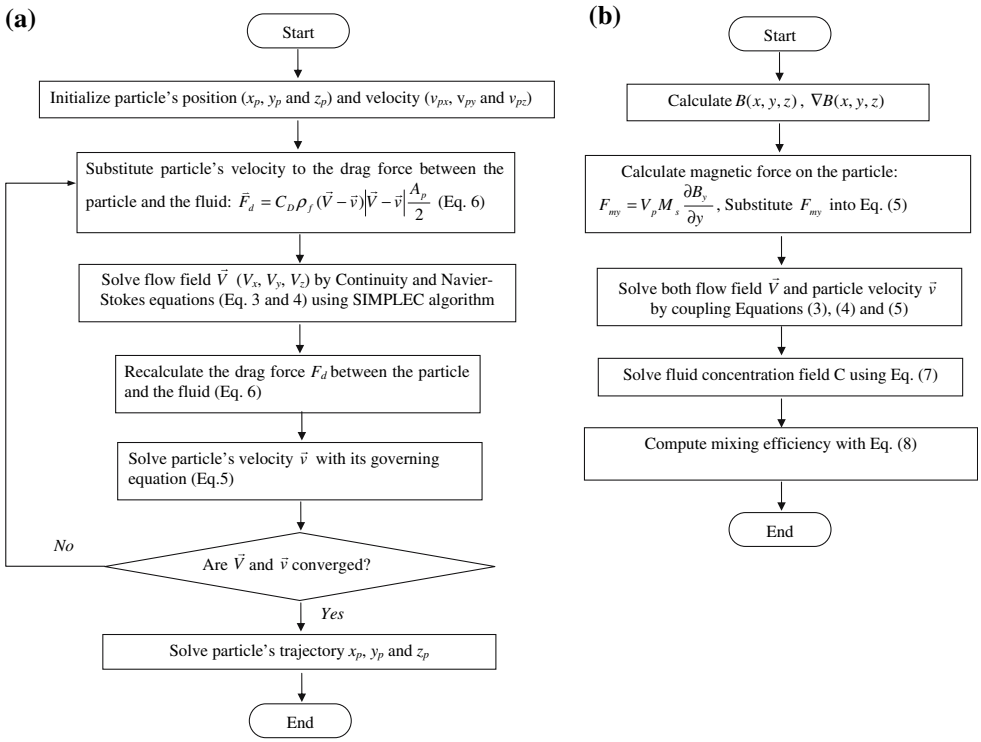

Fig. 5 Flow chart for **a** fluid-particle coupling and **b** magnetic mixing scheme used in this study

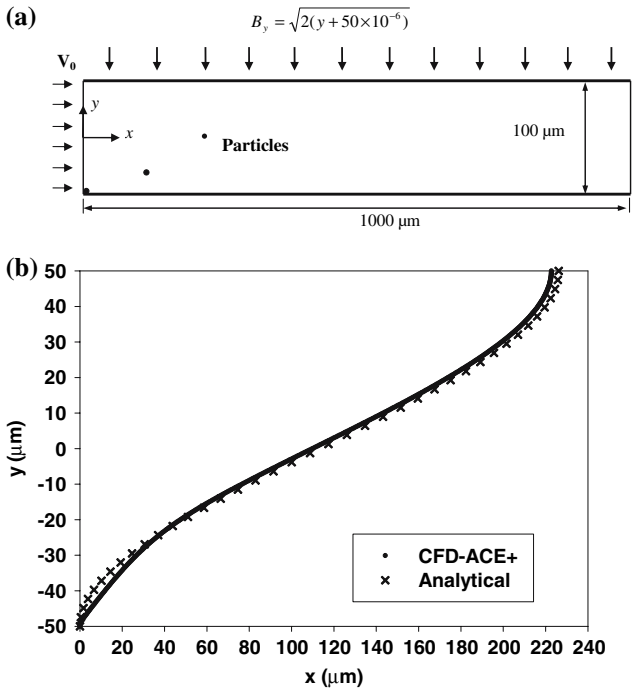

Fig. 6 Numerical model validation: **a** schematic diagram of the 2D microchannel. The particle is initially located at the *left bottom* corner of the microchannel; **b** comparison of particle trajectories obtained by numerical simulation and analytical solution. Particle trajectory is recorded at every 0.2 s

Table 2 Property of the fluid studied in current model

Permeability of free space	μ_0	$4\pi \times 10^{-7}$ N/A^2
Relative permeability of the fluid	μ_r	1.0
Carrier fluid density	ρ_f	1,000 kg/m^3
Carrier fluid dynamic viscosity	η	1×10^{-3} kg/m s

$$V_x(y) = \frac{3}{2} V_0 \left(1 - \frac{4y^2}{W^2}\right). \tag{9}$$

The magnetic force (along the y-direction) and the hydrodynamic drag force (along both x and y directions) on particles are given in Eqs. 10 and 11, respectively:

$$F_{my} = V_p M_y \frac{\partial B_y}{\partial y} = \frac{V_p \chi_p B_y \frac{\partial B_y}{\partial y}}{\mu_0 \mu_r} \tag{10}$$

$$F_{dx} = -6\pi\eta r_p (v_x - V_x) \quad \text{and} \quad F_{dy} = -6\pi\eta r_p (v_y - 0). \tag{11}$$

Here the magnetic particles are not saturated because the applied magnetic field is weak. A linear relationship between its magnetization and external magnetic field is held (shown in Fig. 2). The governing equation for the particles can be decomposed into two parts along different directions:

$$m_p \frac{dv_x}{dt} = F_{dx} = -6\pi\eta r_p (v_x - V_x) \tag{12}$$

$$m_p \frac{dv_y}{dt} = F_{dy} + F_{my} = -6\pi\eta r_p v_y + \frac{V_p \chi_p B_y \frac{\partial B_y}{\partial y}}{\mu_0 \mu_r}. \tag{13}$$

Solutions of Eqs. 12 and 13 lead to the following particle velocity profiles:

$$v_x = v_{x0} e^{-c_1 t} + V_x (1 - e^{-c_1 t}) \tag{14}$$

$$v_y = v_{y0} e^{-c_1 t} + \frac{c_2}{c_1}(1 - e^{-c_1 t}) \tag{15}$$

where $c_1 = 6\pi\ \eta r_p\ /m_p$ and $c_2 = \frac{V_p \chi_p B_y \frac{\partial B_y}{\partial y}}{\mu_0 \mu_r} \Big/ m_p$.

At the beginning ($t = 0$ s), the particle is located at the left corner of the channel wall and hence the particle's velocity v_{x0} and v_{y0} are zero. Based on the afore-mentioned initial conditions, the final particle trajectory is obtained:

$$x = -\frac{2V_0}{W^2}\frac{c_1}{c_2}\left[y_p\left(y_p^2 - \frac{3}{4}W^2\right) - \frac{W^3}{4}\right]. \tag{16}$$

Figure 6b depicts the particle trajectory calculated by Eq. 16.

Simulation of the particle trajectory using CFD-ACE+ has also been conducted. The 2D simulation model utilizes 3,762 cells. It can be seen that during the time period from $t = 0$ s to $t = 0.2$ s, the particle's trajectories predicted by the analytical solution and the numerical model are in good agreement.

Mesh independence test of the numerical scheme was also performed. Four mesh configurations (490, 1,422, 3,762 and 9,522 cells) are tested for this validation problem, and grid-independent results are obtained on the current mesh (3,762 cells). In the micromixer simulation, mesh independence has also been checked. The convergence criteria for all numerical results are set as 1×10^{-6}.

5.2.2 *Comparison to the experimental results*

The numerical scheme presented in Sect. 5.1 was used to study the performance of a micromixer reported by Rida and Gijs (2004a). A schematic of their micromixer is illustrated in Fig. 7a. To simulate their experimental work, 3 μm diameter paramagnetic particles are used in a 5 mm (long) × 200 μm (wide) × 200 μm (high) channel. The time dependent magnetic actuation forces are obtained from two 200 μm wide electromagnet poles. The magnetic particles are agitated in the actuation region ($x = 0$ to $x = 200$ μm). The inlet fluid flow is set at 0.5 cm/s and the magnetic particle flow rate is maintained at 1 μl/s. A square-shaped magnetic agitation field is applied ($f = 5$ Hz, $B_y = 30$ mT at the centerline of the microchannel). These simulation parameters are identical to the experimental conditions of Rida and Gijs (2004a). Note here that in this configuration, the magnetic particles were not saturated because of the small local magnetic field generated between the two poles.

Three-dimensional numerical simulation is performed using the Spray module of CFD-ACE+. The mesh independent results are obtained by using 24,100 cells. The fully developed fluid flow field and the concentration field by diffusion (without particle agitation) in the microchannel are set as the initial conditions for this validation study. Figure 7b shows the simulation results of the concentration distribution across the microchannel at the outlet ($x = 3$ mm) when the mixing reaches stable condition. Our simulation results qualitatively agree with the experimental trend observed by Rida and Gijs (2004a). The fluorescent intensity image reported at their experimental work is presented in Fig. 7c.

In order to show the quantitative matching between the experiments and simulation, the concentration variation along the y direction at $x = 3$ mm is presented in Fig. 7d. The simulation results are in good agreement with the fluorescent measurements. The overall mixing efficiency predicted by the simulation at this location ($x = 3$ mm) is 67%, while the experimental result illustrates a 70% mixing efficiency. The slight difference in the mixing efficiency prediction is possibly due to the measurement uncertainty and the variation in the magnetic particle volume ratio due to the magnetic particle retention effect.

6 Results and discussion

In this section we present the mixing performances of the magnetic mixer shown in Fig. 1a. Parameters considered in this numerical work are applied magnetic force and switching frequency for the electromagnets. Numerical results are obtained based on a 3D model where the dimension normal to the chip substrate (H) is fixed to be 100 μm. For the concentration equation, $D = 10^{-10}$ m^2/s ($Sc = 10^4$) is used in order to obtain appropriate molecular diffusion effects in the species transport equation. In our study, the volume fraction of the particles ranges from 0.019 to 0.057%. With such a low fraction of the particles, the presence of the particles has negligible influence on the fluid properties (Berthier and Silberzan 2006). The mixing performance is evaluated by Eq. 8.

6.1 Effect of magnetic actuation forces

Many factors could affect the micromixing including (1) applied current, (2) geometry of the electromagnet, (3) magnetization M_s of the magnetic particles, (4) size of the

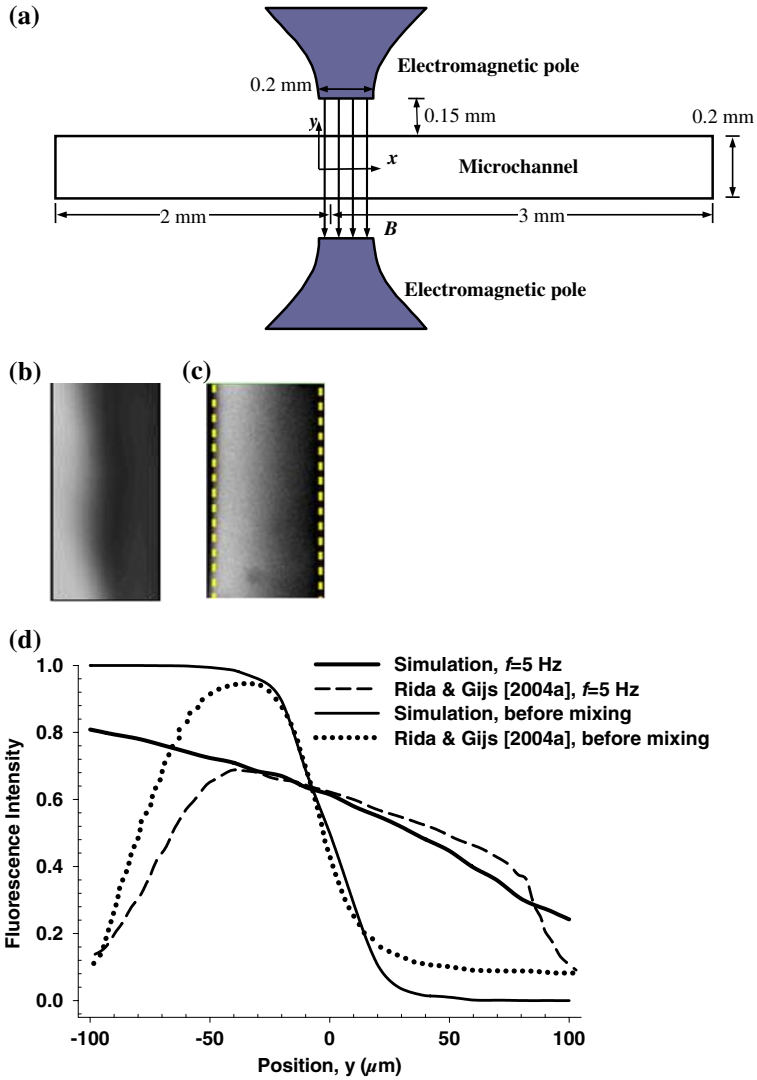

Fig. 7 Comparison to experimental results: **a** schematic diagram of the fluidic structure and the magnetic poles of an electromagnet; **b** simulation result of the fluorescence intensity at the downstream; **c** experimental results of the fluorescence intensity at the same location (Courtesy of Rida and Gijs); **d** comparison of the fluorescence intensity at the channel outlet (x = 3 mm)

magnetic particles, (5) the relative position of the microchannel to the electromagnet. These factors determine the actuation forces on the magnetic particles. Systematic numerical simulations are performed to study the effect of the magnetic actuation forces. The effect of three actuation forces (1.66, 8.27 and 16.6 pN) are investigated. These forces can be generated by applying a current I = 5, 25 and 50 mA to the electromagnet, as shown in Fig. 3b. The switching frequency is set as f = 10 Hz. The particle ratio (volume/volume) is 0.057% for all three cases. Figure 8 shows the numerical solution of the mixing efficiencies at an intermediate position of the microchannel (x = 500 μm). To explain the mixing mechanism due to the magnetic particle agitation, vector field of the fluid flow inside the microchannel is plotted in Fig. 9 under different conditions used in Fig. 8.

For the case of small actuation force (F = 1.66 pN), the mixing efficiency is approximately 32.5% at t = 1 s and 48.6% at t = 2 s. This is because the magnetic forces only allow the magnetic particles to oscillate within a small distance in the lateral direction. Thus only a small fraction of the magnetic particles initially located close to the fluid interface move into the upper half of the channel filled with the buffer solution within a limited area near the interface (see Fig. 9). So the enhancement of the micromixing is limited. It is expected a large magnetic force that can cause the magnetic particles to oscillate within the full channel in the lateral direction will enhance the micromixing. This can be seen from the case where the magnetic actuation force is F_{my} = 8.27 pN, the mixing efficiency reaches 77.6% at 1 s and 98.3% at t = 2 s. With an applied current of 25 mA, the power consumption for the pair of the electromagnets is 0.009 W. Thus rapid mixing can be enabled by this simple configuration. When a magnetic actuation force F_{my} 16.6 pN is applied to the magnetic particles it is found that the mixing performance is degraded, i.e, a longer time is required to achieve a mixing efficiency of approximately

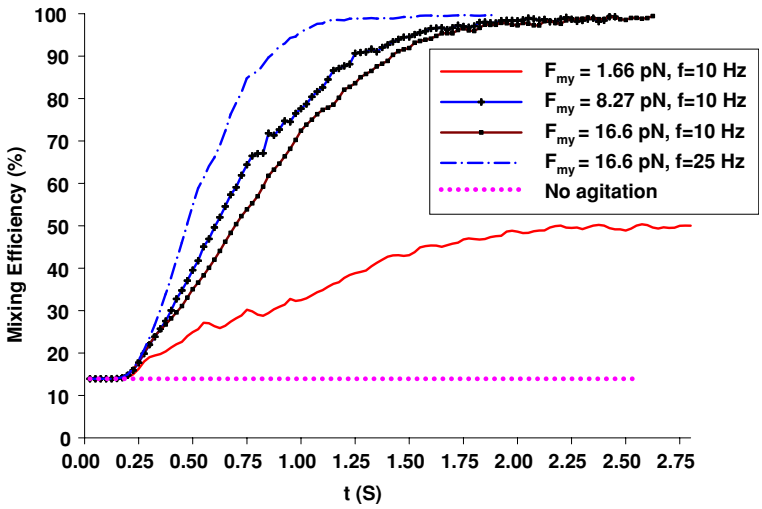

Fig. 8 Effects of the magnetic actuation force on the mixing efficiency at an intermediate position of the micromixer (x = 500 μm). W = 100 μm, Pe = 1,000

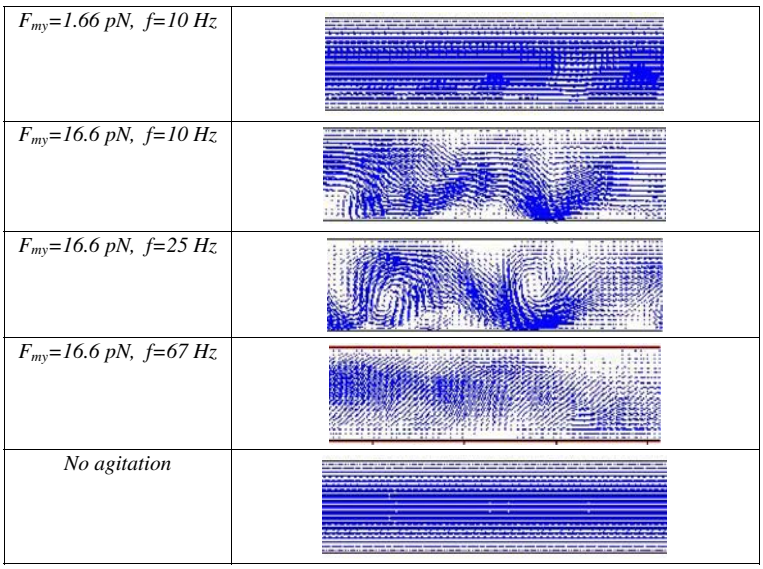

Fig. 9 Velocity vector field in the central plane (z = 0, x = 400–800 μm) of the magnetic micromixer under different magnetic forces and switching frequencies described in Fig. 8. Numerical results are obtained at the moment before the direction of the magnetic force is switched. W = 100 μm, Pe = 1,000

97.2%. This implies that f = 10 Hz is not the optimum switching frequency. We can increase the switching frequency f to speed up the micromixing. As shown in Fig. 8, with a magnetic actuation force of 16.6 pN and a switching frequency of 25 Hz, at x = 500 μm, the mixing efficiency reaches 97.7% within 1.1 s, while it takes 2 s to reach the same mixing efficiency under a switching frequency of 10 Hz. This is because a large actuation force and an increased switching frequency allow more cycles of full-range oscillation of magnetic particles within a fixed time. However, a large switching frequency may not work for small actuation force because of the limited travel velocity in the lateral direction (y-direction). For example, when F_{my} = 1.66 pN, the application of a large switching frequency (f = 10 Hz) does not induce an efficient mixing (see Fig. 8). The above analysis on particle agitation within the microchannel can be seen from the corresponding concentration contour of five cases shown in Fig. 10 at t = 2.0 s. The blue color represents the concentration of the buffer solution and the pink color represents the concentration of the sample solution. For comparison purposes, the concentration contour of no-magnetic-agitation case is also presented. In this case, the micromixing is completely dependent on the diffusion and thus has the lowest mixing efficiency.

The above numerical results imply that the maximum efficiency will be obtained by applying a large magnetic actuation force and an optimal switching frequency. The optimal switching frequency is dependent on the magnetic force, and the desired travel distance of the particles in the lateral direction. The selection of switching frequency will be discussed in the following section.

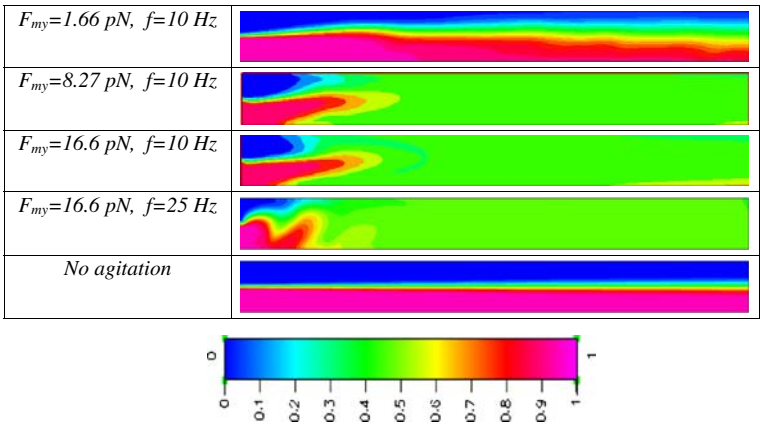

Fig. 10 Concentration contour in the central plane ($z = 0$) of the magnetic micromixer under different magnetic forces and switching frequencies described in Fig. 8. Numerical results are obtained at $t = 2.0$ s. $W = 100$ μm, $Pe = 1{,}000$

6.2 Effects of switching frequency

In the magnetic mixer configuration shown in Fig. 1, alternating magnetic actuating forces (force direction is reversed) on the particles induce particles' oscillations in the microchannel. The particle oscillation brings lateral momentum (in y-direction) to the fluid and stretch/fold streamlines of the fluids. Hence the switching frequency is one critical factor affecting the micromixing. Eight different switching frequencies are considered to optimize the mixing performance in a microchannel with a lateral dimension $W = 100$ μm. In this section, the applied magnetic force is fixed at 16.6 pN when the switching frequency is not zero. The mixing efficiencies at an intermediate position of microchannel ($x = 500$ μm) predicted by the numerical scheme are presented in Fig. 11. For the purpose of comparison, the case with no actuation where particles are not injected into the channel is also plotted in the figure. The mixing efficiency is only 13.9%. Numerical results show that at low switching frequencies ($f = 2$ Hz), the mixing efficiency is quite oscillatory, ranging from 30.9 to 68.9%. This is due to the fact that at a low switching frequency the particles all move to the other half of the channel and bring the surrounding fluid (sample/buffer) to the other fluid (buffer/sample). When the particles reach the channel wall they stay there because of the attractive magnetic forces until the other electromagnet is switched on to generate reverse actuating magnetic force.

To reach an efficient mixing, the electromagnets have to be switched on and off at a higher frequency. Figure 11 shows that at a switching frequency of $f = 10$ Hz, the mixing efficiency reaches 72.4% at $x = 500$ μm at $t = 1$ s, and the mixing becomes stable ($\eta_e = 97.2\%$) at $t = 2$ s. Further increase in the switching frequency f (=14.29, 18.18 Hz) leads to the mixing efficiency of 81.8, 86.5% at $t = 1$ s, and a stable mixing efficiency of 96.9 and 96.6%, respectively, can be achieved at $t = 1.4$ s. At $f = 25$ Hz, a complete mixing ($\eta_e = 97.7\%$) is achieved at approximately $t = 1.1$ s. As we further increase the switching frequency, the effective travel/oscillation range of magnetic particles is reduced in the channel's lateral direction, leading to a longer mixing time. This can be seen from the mixing efficiency curves for $f = 33.33$ Hz and $f = 40$ Hz, where the complete mixing (efficiencies of 97.8 and 96.5%) is achieved at approximately $t = 1.3$ s and $t = 1.35$ s, respectively. While for the optimum switching frequency (25 Hz), the particles can oscillate within the full range of the channel's lateral direction, which is important for mixing the fluid near the wall where the diffusion is negligible. However, at a very high frequency ($f = 100$ Hz), magnetic particles can only oscillate within a very limited range near the fluid interface. The mixing efficiency drastically drops to 41.7% at $x = 500$ μm and $t = 2$ s.

The contour of concentration at different time for the case of $f = 25$ Hz is demonstrated in Fig. 12. At $t \leq 0$, with the absence of agitation of the magnetic particles, the mixing is dominated by the diffusion and the mixing efficiency is very low (13.9% at $x = 500$ μm). At $t > 0$ magnetic particles are injected into the microchannel and are agitated by the time-dependent magnetic field. As shown in Fig. 12, starting at $t = 0.8$ s, complete mixing is already achieved at an intermediate location of the channel ($x = 300$ μm). The average mixing efficiency reaches 94.7% at this position. Then the well-mixed fluid starts to fill in the downstream section, while the magnetic particles continue to oscillate and increase the mixing efficiency in the downstream. These results indicate that the simple micromixing scheme, utilizing alternating magnetic fields, offers a highly efficient mixing within a very short time.

6.3 Critical/optimal switching frequency for magnetic mixing

Because the goal of the magnetic micromixer is to obtain the maximum and stable mixing of the sample and buffer

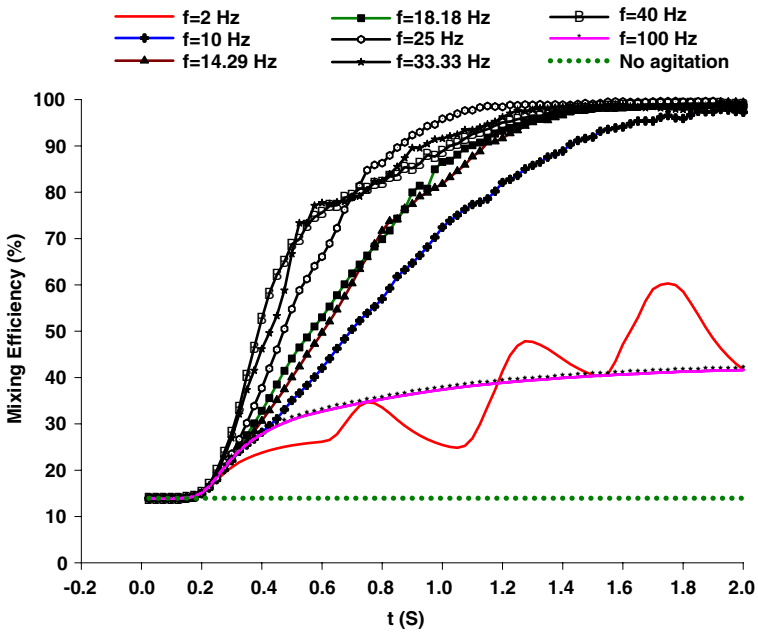

Fig. 11 Mixing efficiency at an intermediate position (x = 500 μm) of the micromixer under different switching frequencies. W = 100 μm and Pe = 1,000

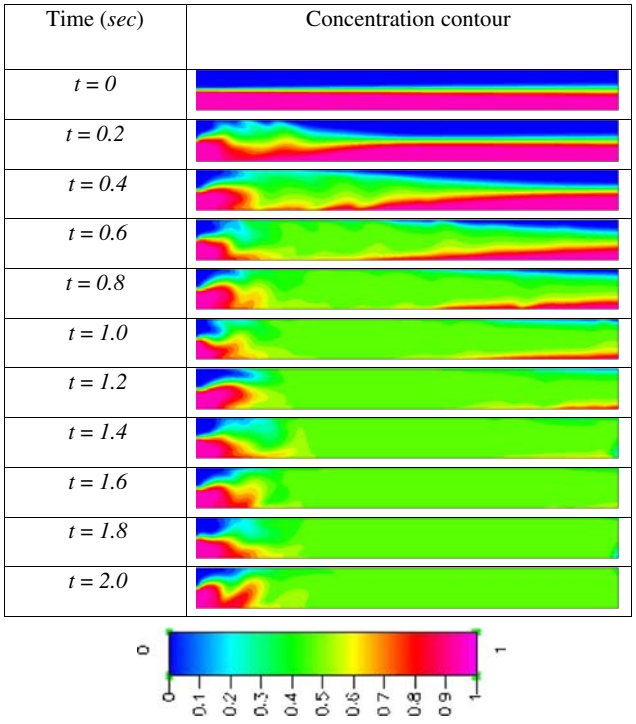

Fig. 12 Concentration contours at different times in the central plane (z = 0) of the mixing channel. W = 100 μm, f = 25 Hz. Initially two fluids are mixed by the diffusion only without agitation by particles

solutions, an appropriate switching frequency (the optimum switching frequency) would be necessary to increase the interfacial areas of those two fluids. There are two factors that affect the maximum frequency: the particle lateral travel velocity (y-direction) and the channel's lateral dimension W. The former is determined by the applied magnetic actuation force. We define the characteristic velocity as the particle's relative velocity, U, when the drag force in the y-direction is balanced by the magnetic actuation force. From Stokes' equation, the drag force can be written as:

$$F_d = -6\pi\eta r_p(v_y - V_y) = -6\pi\eta r_p U$$

where v_y and V_y are particle's and fluid's velocities in y direction, respectively, η is the dynamic viscosity of the fluid, U is the relative velocity, $U = v_y - V_y$

The relative velocity (U) can be obtained from the force balance as

$$U = \frac{F_{my}}{6\pi\eta r_p} \tag{17}$$

where F_{my} can be calculated by Eq. 2. Using this characteristic velocity, we introduce the critical switching frequency as

$$f_{cr} = \frac{U}{W} \tag{18}$$

where W is the channel's lateral dimension.

Under the present conditions, the above characteristic velocity and corresponding critical frequency are calculated and listed in Table 3.

The average mixing efficiency at an intermediate location (x = 500 μm) of the microchannel for different switching frequency is presented in Fig. 13. Numerical results of the optimal switching frequency appear consistent with Eq. 18. Note that the optimum switching fre-

Table 3 Characteristic velocity and critical frequency prediction for different channels

Channel's lateral dimension W (μm)	Characteristic velocity U (mm/s)	Critical frequency f_{cr} (Hz)
100	1.756	17.56
300	1.756	5.85

quency is defined as the frequency for which the average mixing efficiency is the maximum. The average mixing efficiency is calculated by integrating the mixing efficiency over one switching cycle, i.e., $\bar{\eta}_e = \frac{\int_{t_1}^{t_1+T} \eta_e(t)dt}{T}$, where $T = 1/f$, t_1 is an arbitrary moment after a repeatable fluid pattern is reached. When the mixing efficiency does not show repeated patterns, T should be replaced by several cycles, nT, (n = 1, 2, 3...) to obtain an average value. The error bars in Fig. 13 indicate the oscillation range of the mixing efficiency. Numerical work on the mixer performance on a microchannel with lateral dimension W = 300 μm was also conducted to find the optimal frequency. The other dimensions and conditions including number of particles injected into the channel per switching cycle are kept the same as those of the 100 μm wide channel. The average mixing efficiency vs. switching frequency is also shown in Fig. 13. Four frequencies, f = 4, 5.88, 12.5 Hz and 66.67 Hz are considered for this case. The optimum switching frequency provided by the numerical scheme for the cases of W = 100 μm and W = 300 μm, as shown in Fig. 13, is 25, and 5.88 Hz, respectively, while Eq. 18 suggests 17.56 and 5.85 Hz. It is obvious that the increase of channel's lateral dimension W shifts the optimal switching frequency to a lower level. It can be also predicted from Eq. 18 that the application of a larger magnetic force (i.e. increase the applied current) will shift the optimal frequency to a high level because it increases the particle travel velocity along the channel's lateral direction. We noticed that the average mixing efficiency is lower for the microchannel with lateral dimension of 300 μm. This is because as we increase the channel's lateral dimension (thus the flow rate) while injecting the same number of magnetic particles, the volume fraction of particles in this case is 0.019%. Thus there are fewer particles per volume that agitate and disturb the fluid flow, the key factor to enhance the micromixing.

It can be seen from Fig. 13 that the maximum mixing efficiency occurs at approximately an optimum switching frequency of $f_{cr} = U/W$. Figure 14 shows the mixing efficiency dependence on Strouhal number [$St = Wf/U = (f/f_{cr})$]. The solid line is based on a fourth-order polynomial curve fit of the numerical data points. It is seen that the maximum mixing efficiency occurs at St = 1. We should

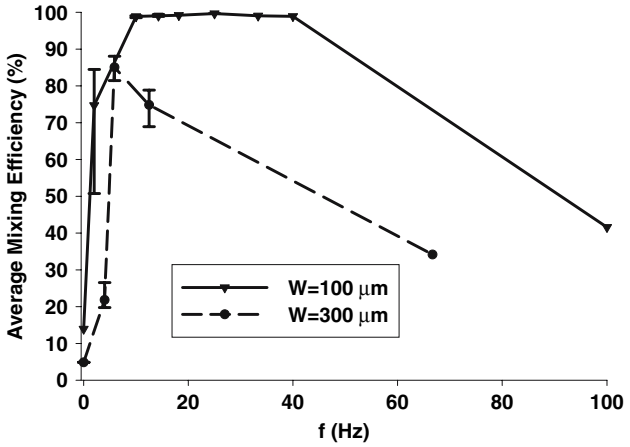

Fig. 13 Average mixing efficiency at an intermediate position (x = 500 μm) of the magnetic micromixer for different electromagnetic switching frequencies. Each error bar indicates the oscillation range of the mixing efficiency. The data points on the curves are the average values calculated by integrating mixing efficiency over a switching cycle (or several cycles). The optimum frequency for micromixers with lateral dimension W = 100 μm and 300 μm are 17.56 and 5.85 Hz, respectively

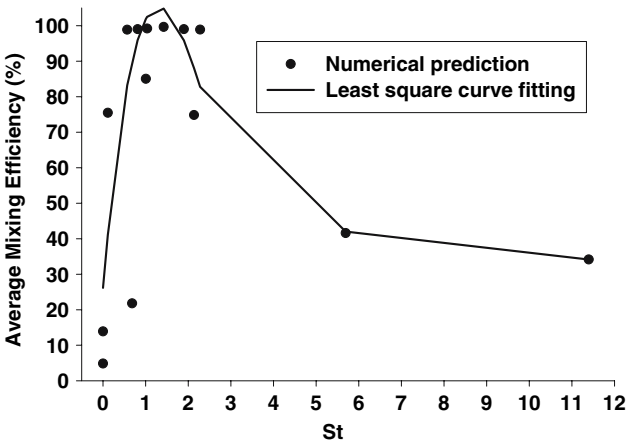

Fig. 14 Mixing efficiency variation with Strouhal number (St). The optimum mixing efficiency takes place at $St \approx 1$

note here that Eq. 18 only provides an appropriate prediction of optimum frequency for magnetic micromixers in a straight channel. Because of the complexity involved in the coupling of the fluid flow and magnetic particles, it may not be accurate to use Eq. 18 to estimate the particle travel velocity along the y-direction. This is especially true for a microchannel with complicated geometries that further complicates flow patterns and particle motions, and hence the optimum frequency. Nevertheless, numerical results indicate that a switching frequency close to the critical switching frequency ($St \approx 1$), the high mixing efficiency is expected to achieve.

7 Conclusions

Effective mixing of sample solutions containing magnetic beads and biological solutions are critical for the microfluidic devices targeted at micro biological assay systems. Rapid mixing can reduce the analysis time and permit high throughput in lab-on-a-chip devices. We presented the numerical work for a magnetic micromixer consisted of a microchannel and a pair of electromagnets.

The effects of various design parameters such as applied magnetic actuation forces and operating frequency have been studied. For micromixer utilizing magnetic particle agitation, the critical (optimum) switching frequency depends on the channel's lateral dimension and the applied magnetic force. For a large magnetic actuation force, the micromixer needs to be operated with a higher operating frequency to obtain the maximum mixing efficiency. For wider microchannels, the maximum efficiency is obtained at a relatively low actuation frequency. If the magnetic particles are actuated with a much lower frequency, particles move to one direction and stay on the wall until the magnetic forces are reversed; as a result, they tend to add limited agitation to the fluid flow. While at much higher operating frequency, the magnetic particles only oscillate in a narrow range and do not enhance the micromixing significantly. The optimum switching frequency obtained from the present numerical prediction is in good agreement with the theoretical analysis.

Numerical results also illustrate that such a simple micromixer configuration is sufficient for a complete micromixing within a short distance and time, with no need to fabricate complex serpentine channels. At the optimal switching frequency range, a high mixing efficiency (97.7%) can be achieved within 1.1 s at $x = 500$ μm for a particle ratio of 0.057% and the 100 μm wide channel, while the applied current to the electromagnet is 50 mA.

Acknowledgments This work was partially supported by NSF grant# 0708540 and a University of Akron Faculty Research Summer Fellowship. The authors thank Dr. Tsukerman in the Department of Electrical and Computer Engineering of the University of Akron for the helpful discussion on the magnetic force calculation.

References

ASM Committee on Magnetically Soft Materials (1964) Metals handbook: magnetically soft materials, 8th edn, vol 1. American Society for Metals, Metals Park, OH, p 792

Berthier J, Silberzan P (2006) Microfluidics for biotechnology. Artech House 134:288–289

Bessoth FG, DeMello AJ, Manz A (1999) Microstructure for efficient continuous flow mixing. Anal Commun 36:213–215

Biddiss E, Erickson D, Li D (2004) Heterogeneous surface charge enhanced micro-mixing for electrokinetic flows. Anal Chem 76:3208–3213

Bottausci F, Mezic I, Meinhart CD, Cardonne C (2004) Mixing in the shear superposition micromixer: three-dimensional analysis. Philos Trans R Soc Lond A 362:1001–1018

Bouteville A (2005) Numerical simulation applied to chemical vapor deposition process, rapid thermal CVD and spray CVD. J Optoelectron Adv Mater 7:599–606

Crocker DS, Presser C, Widmann JF (2001) CFD modeling and comparison with data for the NIST reference spray combustor. In: ASME international mechanical engineering conference and exhibition, November 11–16, New York, NY

Deval J, Tabeling P, Ho CM (2002) A dielectro-phoretic chaotic mixer. In: Proc. of the 15th IEEE international conference on MEMS, pp 36–39

Furlani EP (2001) Permanent magnet and electromechanical devices. Academic, New York, p 135

Gijs MAM (2004) Magnetic bead handling on-chip: new opportunities for analytical applications. Microfluid Nanofluid 1:22–40

Hayes MA, Polson NA, Phayre AN, Garcia AA (2001) Flow-based microimmunoassay. Anal Chem 73:5896–5902

Hessel V, Lowe H, Schonfeld F (2005) Micromixers-a review on passive and active mixing principles. Chem Eng Sci 60:2479–2501

Hong CC, Choi JW, Ahn CH (2004) A novel in-plane passive microfluidic mixer with modified tesla structures. Lab Chip 4:109–113

Jacobson SC, McKnight TE, Ramsey JM (1999) Microfluidic devices for elctrokinetically driven parallel and serial mixing. Anal Chem 71:4455–4459

Liu RH, Yang J, Pindera MZ, Athavale M, Grodzinski P (2002) Bubble-induced acoustic micromixing. Lab Chip 2:151–157

Losey MW, Jackman RJ, Firebaugh SL, Schmidt MA, Jensen KF (2002) Design and fabrication of microfluidic devices for multiphase mixing and reaction. J Microelectromech Syst 11:709–717

Lu LH, Ryu KS, Liu C (2002) A magnetic microstirrer and array for microfluidic mixing. J Microelectromech Syst 11:462–469

McClain MA, Culbertson CT, Jacobson SC, Ramsey JM (2001) Flow cytometry of escherichia coli on microfluidic devices. Anal Chem 73:5334–5338

Mengeaud V, Josserand J, Girault HH (2002) Mixing processes in a zigzag microchannel: finite element simulations and optical study. Anal Chem 74:4279–4286

Nguyen NT, Wu ZG (2005) Micromixers-a review. J Micromech Microeng 15:R1–R16

Oddy MH, Santiago JG, Mikkelsen JC (2001) Electrokinetic instability micromixing. Anal Chem 73:5822–5832

Pamme N (2006) Magnetism and microfluidics. Lab chip 6:24–38

Rida A, Gijs MAM (2004a) Manipulation of self-assembled structures of magnetic beads for microfluidic mixing and assaying. Anal Chem 76:6239–6246

Rida A, Gijs MAM (2004b) Dynamics of magnetically retained supraparticle structures in a liquid flow. Appl Phys Lett 85:4986–4988

Rong R, Choi JW, Ahn CH (2003) A functional magnetic bead/biocell sorter using fully integrated magnetic micro/nano tips. In: IEEE 16th international conference on MEMS (MicroElectroMechanical Systems), January, Japan, pp 530–533

Ryu KS, Shaikh K, Goluch E, Fan ZF, Liu C (2004) Micro magnetic stir-bar mixer integrated with parylene microfluidic channels. Lab Chip 4:608–613

Santiago JG (2001) Electroosmotic flows in microchannels with finite inertial and pressure forces. Anal Chem 73:2353–2365

Suzuki H, Ho CM, Kasagi N (2004) A chaotic mixer for magnetic bead-based micro cell sorter. J Microelectromech Syst 13:779–790

Tsai JH, Lin L (2002) Active microfluidic mixer and gas bubble filter driven by thermal bubble micropump. Sens Actuators 97–98:665–671

Wang Y, Zhe J, Dutta P, Chung BTF (2007) A microfluidic mixer utilizing electrokinetic relay switching and asymmetric flow geometries. J Fluids Eng 129:395–403

West J, Karamata B, Lillis B, et al (2002) Application of magneto-hydrodynamic actuation to continuous flow chemistry. Lab Chip 2:224–230

Xuan X, Li D (2005) Electroosmotic flow in microchannels with arbitrary geometry and arbitrary distribution of wall charge. J Colloid Interface Sci 289:291–303

Yang Z, Matsumoto S, Goto H, Matsumoto M, Maeda R (2001) Ultrasonic micromixer for microfluidic systems. Sens Actuators 93:266–272

Zborowski M, Sun LP, Moore LR (1999) Continuous cell separation using novel magnetic quadrupole flow sorter. J Magn Magn Mater 194:224–230

Zolgharni M, Azimi SM, Bahmanyar MR, Balachandran W (2007) A numerical design study of chaotic mixing of magnetic particles in a microfluidic bio-separator. Microfluidics Nanofluidics. doi:10.1007/s10404-007-0160-9